Redox Biology 55 (2022) 102399

Contents lists available at ScienceDirect

Redox Biology

journal homepage: www.elsevier.com/locate/redox

Cytoglobin inhibits non-thermal plasma-induced apoptosis in melanoma cells through regulation of the NRF2-mediated antioxidant response

Joey De Backer [a,d,*], Abraham Lin [b,c], Wim Vanden Berghe [a,1], Annemie Bogaerts [b,1], David Hoogewijs [d,1]

[a] Protein Chemistry, Proteomics and Epigenetic Signaling (PPES) Research Group, Department of Biomedical Sciences, University of Antwerp, Belgium
[b] Plasma Lab for Applications in Sustainability and Medicine-Antwerp (PLASMANT) Research Group, Department of Chemistry, University of Antwerp, Belgium
[c] Center for Oncological Research (CORE), Integrated Personalized & Precision Oncology Network (IPPON), University of Antwerp, Belgium
[d] Section of Medicine, Department of Endocrinology, Metabolism and Cardiovascular System, University of Fribourg, Switzerland

ARTICLE INFO

Keywords:
Melanoma
Cytoglobin
Non-thermal plasma
ROS
Apoptosis

ABSTRACT

Melanoma arises from pigment-producing cells called melanocytes located in the basal layers of the epidermis of the skin. Cytoglobin (CYGB) is a ubiquitously expressed hexacoordinated globin that is highly enriched in melanocytes and frequently downregulated during melanomagenesis. Previously, we showed that non-thermal plasma (NTP)-produced reactive oxygen and nitrogen species (RONS) lead to the formation of an intramolecular disulfide bridge that would allow CYGB to function as a redox-sensitive protein. Here, we investigate the cytotoxic effect of indirect NTP treatment in two melanoma cell lines with divergent endogenous CYGB expression levels, and we explore the role of CYGB in determining treatment outcome. Our findings are consistent with previous studies supporting that NTP cytotoxicity is mediated through the production of RONS and leads to apoptotic cell death in melanoma cells. Furthermore, we show that NTP-treated solutions elicit an antioxidant response through the activation of nuclear factor erythroid 2–related factor 2 (NRF2). The knockdown and overexpression of CYGB respectively sensitizes and protects melanoma cells from RONS-induced apoptotic cell death. The presence of CYGB enhances heme-oxygenase 1 (HO-1) and NRF2 protein expression levels, whereas the absence impairs their expression. Moreover, analysis of the CYGB-dependent transcriptome demonstrates the tumor suppressor long non-coding RNA maternally expressed 3 (MEG3) as a hitherto undescribed link between CYGB and NRF2. Thus, the presence of CYGB, at least in melanoma cells, seems to play a central role in determining the therapeutic outcome of RONS-inducing anticancer therapies, like NTP-treated solutions, possessing both tumor-suppressive and oncogenic features. Hence, CYGB expression could be of interest either as a biomarker or as a candidate for future targeted therapies in melanoma.

1. Introduction

Skin cancer is the most common cancer in the United States and the 19th most common worldwide [1]. Of all types of skin cancers, melanoma has the lowest incidence rate, with only 1% of skin cancers diagnosed being melanoma. However, melanoma (especially metastatic malignant melanoma) causes most of the skin cancer deaths with a 5-year survival of 20% [1]. Recent advancements in targeted and immunotherapy for melanoma have offered drastic improvements in survival to some patients, but most patients fail to have a sustained response.

Solar ultraviolet radiation (UVR) is considered to be the main etiological factor for melanomagenesis [2]. UVR comprises ultraviolet C (UVC; 200–290 nm), ultraviolet B (UVB; 290–320 nm), and ultraviolet A (UVA; 320–400 nm), with the latter two constituting the main effectors of skin damage [3]. UV can induce DNA damage through direct as well as mediated mechanisms [4]. UVB exposure directly leads to the generation of DNA photoproducts, DNA strand breaks, and DNA crosslinks. On the other hand, UVA is mostly responsible for oxidative stress-induced DNA damage [5].

Abbreviations: NTP, non-thermal plasma; pPBS, plasma-treated phosphate buffered saline; CYGB, human cytoglobin; RONS, reactive oxygen and nitrogen species.

* Corresponding author. Universiteitsplein 1, 2610, Wilrijk, Belgium.
E-mail address: Joey.debacker@uantwerpen.be (J. De Backer).

[1] Equal senior authorship.

https://doi.org/10.1016/j.redox.2022.102399
Received 25 June 2022; Accepted 5 July 2022
Available online 14 July 2022

Melanoma arises from pigment-producing cells called melanocytes located in the basal layers of the epidermis of the skin. Melanocytes play a very important role in the response to UVR via melanin synthesis [6]. Melanin produced in specialized organelles called melanosomes is transferred to keratinocytes (mediated by multiple keratinocyte-produced paracrine factors) where they protect nuclear DNA from UV irradiation, thereby preventing the generation of DNA damage [7,8]. However, melanin synthesis involves oxidation reactions generating superoxide anion (O_2^-) and hydrogen peroxide (H_2O_2), which subjects melanocytes to increased levels of intracellular reactive oxygen species (ROS) [9,10]. The balance between the pro-oxidant and anti-oxidant properties of melanin are dependent on the redox state of the melanocytes, the relative eumelanin and pheomelanin contents, the levels of melanin intermediates, and the presence of reactive metals within the melanosome microenvironment [11,12]. There is increasing evidence concerning the significance of oxidative stress in the initiation and progression of melanoma, supported by findings that mutations in several melanoma-associated genes result from, or exacerbate, oxidative stress [10,13–15].

To maintain redox homeostasis melanocytes possess a highly efficient antioxidant network comprising of both enzymatic (e.g. superoxide dismutase (SOD), catalase (CAT), glutathione peroxidase (GPx), glutathione reductase (GR), and thioredoxin reductase (TR)) and non-enzymatic (e.g. ascorbic acid, glutathione) antioxidants, along with various antioxidant genes, including heme-oxygenase 1 (HO-1), ferritin, and master regulator of the antioxidant response−nuclear factor erythroid 2–related factor 2 (NRF2) [16–19].

Cytoglobin (CYGB) is a ubiquitously expressed hexacoordinated globin recently found to be highly enriched in melanocytes, and frequently downregulated during melanomagenesis [20]. Although the mechanism remains enigmatic, CYGB is thought to play a role in the cellular response towards oxidative stress [21–25]. In melanocytes, highly enriched CYGB may act as a ROS scavenger, protecting the cell from oxidative damage [20]. In melanoma, the transition from melanocytes is frequently, but not always, accompanied by a loss of CYGB expression. Modulation of CYGB expression levels during melanocyte-to-melanoma transition may influence tumor malignancy and the efficacy of cancer treatments.

Non-thermal plasma (NTP) and its biomedical applications have recently become a major focus of research [26–28]. One of the most exciting and extensively studied application is the treatment of cancer [29,30]. NTP consists of a mixture of various components, including charged particles (ions, electrons), reactive neutral species (reactive oxygen and nitrogen species; RONS), UV radiation, and electromagnetic fields [31,32]. Of those, RONS are hypothesized to mediate the effects observed in biological systems as they are known to be involved in rapid reactions with important biomolecules such as proteins, lipids, and nucleic acids [21,33,34]. In recent years, multiple studies have shown that plasma is able to effectively kill many types of cancer cells via different cell death mechanisms, including melanoma [35–39]. NTP can exert its biomedical effects either by direct treatment of cancer cells or by indirect treatment, i.e., by applying NTP-treated solutions, rich in long-lived reactive species [39,40].

Previously, our group has shown that NTP-generated RONS induced an altered conformation of recombinant CYGB, supporting the role of redox-sensitive protein [21]. Although many studies have demonstrated the efficacy of NTP treatment for melanoma, the potential influence of the presence or absence of CYGB in melanoma cells on NTP treatment outcome remains unknown. In this study, different melanoma cell lines, containing abundant or low endogenous CYGB expression levels, were treated indirectly through incubation with phosphate buffered saline (PBS), treated with a non-thermal plasma jet (kINPen IND) for several treatment times. After treatment, cell viability was assessed by flow cytometry, and intracellular ROS concentration was determined using fluorescent probes. CYGB mRNA and protein expression was assessed by real-time quantitative PCR (qPCR) and immunoblotting, respectively. Additionally, CYGB-overexpressing and CYGB-knockdown cells were generated to investigate the influence of CYGB on sensitivity to NTP-treatment. Finally, the CYGB-dependent transcriptome was analyzed.

2. Experimental

2.1. Cell culture

Human A375 (ATCC CRL-1619) and G361 (ATCC CRL-1424) melanoma cells were maintained in Dulbecco's Minimum Essential Media (DMEM) (Gibco, Life Technologies), containing L-Glutamine, supplemented with 10% heat-inactivated fetal bovine serum (FBS, Gibco, Fisher Scientific), and 1% Penicillin/Streptomycin (10,000 Units/mL P; 10,000 μg/mL S; Gibco, Life Technologies). Both cell lines were incubated in a humidified 5% CO_2 atmosphere at 37 °C and were routinely subcultured after trypsinization.

2.1.1. Generation of stable knock-down and overexpression cell lines

Expression vectors encoding short hairpin RNA (shRNA) sequences targeting human CYGB in a pLKO.1-puro plasmid were purchased from Sigma-Aldrich (shCYGB: order number TRCN0000059378). Control cells (shCTR) were transfected with a non-targeting control shRNA under the control of a U6 promoter in a pKLO.1 puromycin resistance vector (Sigma-Aldrich) as described previously [41]. Viral particles were produced in HEK293T cells by co-transfection of the respective transfer vector (3 μg) with the packaging plasmids pLP1 (4.2 μg), pLP2 (2 μg) and pVSV-G (2.8 μg, all from Invitrogen) using $CaCl_2$ transfection as described before [42]. Malme-3M cells were transduced with lentiviral-pseudotyped particles and cell pools were cultured in DMEM supplemented with 10% FBS and 1% Penicillin/Streptomycin with the appropriate antibiotic for selection. For stable overexpression in A375 cells full-length human *CYGB* gene and control gene β-glucuronidase *(GUS)* were cloned into a pLENTI6 plasmid. Viral particles were produced as described above.

2.2. Plasma setup and treatment

Plasma was generated by using the kINPen IND plasma jet (Neoplas GmbH) [43]. Plasma was sustained at an operating frequency of 1 MHz, using argon as a feed gas. The applied gas flow rate and gap distance (nozzle end to surface of solution) were set at 1 L/min, and 10 mm, respectively. For the generation of an NTP-treated solution, 1x PBS was used. In a 12-well plate, 2 mL 1x PBS was treated for 5, 7, or 9 min. Depending on the experiment, plasma-treated PBS (pPBS) was added to cells cultured in complete DMEM in a 1:3 ratio (sections 2.3, 2.6, 2.7, 2.8) or 1:5 ratio (sections 2.4 and 2.5). In NTP-treated solutions, long-lived RONS H_2O_2, NO_2^- and NO_3^- have already been extensively described as the three main effectors of the cytotoxic and genotoxic effects observed in cancer cells, as other short-lived species are quenched very rapidly [35,44,45]. Fluorometric quantification of the concentration of H_2O_2 in pPBS with different treatment times demonstrated the linear treatment time-dependent generation of H_2O_2 in pPBS (Fig. S4).

2.3. Fluorometric hydrogen peroxide assay

The concentration of H_2O_2 was quantified using the fluorometric hydrogen peroxide assay (Sigma-Aldrich) according to the manufacturer's protocol. This kit utilizes a peroxidase substrate that generates an infra-red fluorescent product (λex = 640/λem = 680 nm) after reaction with hydrogen peroxide that can be analyzed by a fluorescent microplate reader. Immediately after NTP treatment, 50 μL pPBS was added to a black clear bottom 96 well plate (Corning). An equal amount of the assay's Master Mix was added to each pPBS containing well. After 30 min incubation in the dark the fluorescence intensity was measured on the Spark Cyto (Tecan). Concentrations were calculated using a H_2O_2

standard.

2.4. Viability and apoptotic cell death

Cell viability and the presence of apoptosis was determined using the FITC-Annexin V (BD Pharmingen) dye in conjunction with the vital dye propidium iodide (PI, Invitrogen) to allow the detection of early apoptotic cells (PI negative, FITC Annexin V positive). The day before treatment 4×10^4 cells were seeded in a 24-well plate, containing complete DMEM. The next day, cells were treated (described in section 2.2) and incubated for 24 h in a humidified 5% CO_2 atmosphere at 37 °C. Cells were collected in round-bottom polystyrene tubes (Falcon), washed (FACS buffer; 1x PBS, 3% FBS, 1 mM ethylenediaminetetraacetic acid (EDTA)) and centrifuged for 5 min at 1500 rpm before being resuspended in ice-cold 1x Annexin V binding buffer (BD Pharmingen). Finally, 1x FITC annexin V was added to the suspension. PI (500 ng) was added right before measuring on the CytoFLEX flow cytometer (Beckman Coulter). Data was analyzed using FlowJo software (FlowJo, BD).

2.5. Caspase activity

The IncuCyte Caspase 3/7 green dye (Sartorius) was used to determine the activation of essential mediators of apoptosis caspases 3 and 7. The IncuCyte Caspase 3/7 Dye is specially formulated for use in the IncuCyte Live-Cell Analysis System (Sartorius). Cells (3×10^3) were seeded in a 96-well plate containing complete DMEM the day before treatment. 30 min before adding pPBS, 5 μM Caspase 3/7 green dye was added to each well. In addition, 1 h prior to treatment, 1 mM of *N*-acetyl cysteine (NAC) was added to some cells. After treatment the plate was incubated in the IncuCyte and images were taken every 2 h over a period of 24 h. Data were analyzed with the IncuCyte ZOOM version 2016B (Essen BioScience) to collect the total green object count per well, defined as the number of apoptotic cells per well.

2.6. Intracellular ROS

To determine the intracellular ROS, CellROX Green Reagent (Invitrogen) was used. The cell-permeant dye is weakly fluorescent while in a reduced state and exhibits bright green photostable fluorescence upon oxidation and subsequent binding to DNA. Cells (3×10^3) were seeded in a 96-well plate containing complete DMEM the day before treatment. 30 min before adding pPBS, 2.5 μM CellROX Green Reagent was added to each well. In addition, 1 h prior to treatment, 1 mM of NAC was added to some cells. After treatment the plate was incubated in an IncuCyte device and images were taken every 2 h over a period of 24 h. Data were analyzed with the IncuCyte ZOOM version 2016B (Essen BioScience) to collect the average green object mean intensity of each well.

2.7. RNA extraction, purification, and cDNA conversion

RNA extraction and purification was performed using a PureLink RNA Mini Kit (Invitrogen), according to the manufacturer's instructions. RNA concentration and purity was measured with an Epoch spectrophotometer (BioTek) by measuring absorbance at 260/280 nm ratio. cDNA was reverse transcribed using Superscript II reverse transcriptase (Invitrogen) according to the manufacturer's protocol.

2.8. Real-time quantitative PCR

Amplification of cDNA and subsequent quantification was performed using the StepOne Real-Time PCR system (Applied Biosystems) using a Power SYBR Green Master Mix (Applied Biosystems). The following conditions were used during PCR: 95 °C for 10 min and 40 cycles of: 95 °C for 15 s; 60 °C for 1 min. All PCR-reactions were performed in duplicate for three biological replicates. Where needed, an inter-run calibrator (IRC) to detect and remove inter-run variation between the different mRNA quantification runs was used. Results were subsequently analyzed using qbase + software (version 3.2, Biogazelle) as described before [46]. A list of used reference and target genes, together with their primer sequences, amplification efficiency, and amplicon size is given in Table S1. All primers were manufactured and provided by Eurogentec or Microsynth.

2.9. Protein extraction and quantification

Lysis buffer, containing 10 mM Tris HCl (pH 8), 1 mM EDTA, 400 mM NaCl, 1% NP-40 and protease inhibitors (Sigma-Aldrich) was used to lyse cells as described before [41]. Lysed cells were placed on a rotating arm at 4 °C for 30 min to allow optimal performance of the lysis buffer. The suspension was subsequently sonicated for 1 min at 60 Hz to degrade any potential formed DNA-aggregates. Finally, samples were centrifuged at 10,000 g for 15 min and the protein-containing supernatant was collected. Protein concentrations were determined using the BCA Protein Assay Kit (ThermoFisher Scientific).

2.10. Immunoblotting

Extracted proteins for immune-based western blotting were first separated, according to molecular weight, using sodium dodecyl sulphate polyacrylamide gel-electrophoresis (SDS-PAGE) gels, followed by electrotransfer to nitrocellulose membranes (Amersham Hybond-ECL, GE Healthcare) as described before [47,48]. Equal amounts of protein and volume were loaded onto a 12.5% polyacrylamide gel for CYGB, heme oxygenase 1 (HO-1), and NF E2 related factor 2 (NRF2). Membranes were blocked in TBS-T (Tris-buffered Saline; 0.1% Tween-20), containing 5% non-fat dry milk, for 1 h at room temperature. After blocking, membranes were incubated overnight at 4 °C with primary antibodies (anti-CYGB, Proteintech, 13317-1-AP; anti--β-2-Microglobulin (B2M), Proteintech, 13511-1-AP; anti–HO–1, Proteintech, 10701-1-AP; anti-NRF2, Proteintech, 16396-1-AP). The following day, membranes were washed with TBST-T, and incubated during 1 h with horseradish-conjugated secondary antibodies (anti--rabbit IgG HRP, Sigma, GENA934-1 ML). The signal was revealed using ECL Prime (Amersham, GERPN2232) on a C-DiGit® Western blot scanner (LI-COR Biosciences) and exported and quantified using Image Studio™ program (LI-COR Biosciences).

2.11. RNA sequencing

Total RNA sample quality was assessed with TapeStation (Agilent Technologies, Santa Clara, CA, USA) and Qubit assay (Invitrogen). Total RNA samples with an RNA integrity number (RIN) > 7.0 and purity (OD_{260}/OD_{280}) ratio 1.8–2.2 were used for subsequent experiments. Sequence libraries were generated using the poly(A) RNA selection method and sequenced by GENEWIZ (Azenta Life Sciences). An independent library was constructed for each of the triplicate samples. High throughput RNA sequencing (RNA-seq) was performed with pair end 150 bp reading length on an Illumina NovaSeq 6000 (Illumina, San Diego, CA) sequencer. The DESeq2 analysis was used to estimate variance-mean dependence and test for differential expression [49]. Genes with a p-adjusted value ≤ 0.05 were considered differentially expressed. Genes with a p-adjusted value ≤ 0.05 and an absolute $\log_2$ fold change ≥ 1 were recognized as significantly differentially expressed genes (DEGs). Volcano plots were generated using the EnhancedVolcano R package to usefully visualize the results of the differential expression analyses.

2.12. Glutathione assay

Total cellular glutathione (GSH) levels were detected using the luminescence-based GSH-Glo Glutathione Assay (Promega), according to the manufacturers protocol. The assay is based on the conversion of a

luciferin derivative into luciferin in the presence of glutathione, catalyzed by glutathione S-transferase (GST). Briefly, 5000 A375-GUS, A375-hCYGB, G361-shCTR, and G361-shCYGB cells were seeded out in a white opaque 96-well microplate (PerkinElmer). The next day, cells were either untreated, treated with 1 mM NAC only, or pre-treated with 1 mM NAC 1 h before pPBS treatment. After 6 h, luminescence was measured using the Spark Cyto (Tecan). GSH concentrations were calculated using a GSH standard curve.

2.13. Statistical analysis

The data are presented as the mean ± standard error of the mean (SEM). The statistical tests were performed with Prism GraphPad software. Flow cytometric viability data was assessed for statistical significance using one-way ANOVA followed by Tukey's multiple comparison test. Statistically significant differences compared to the untreated control were visually represented in the figures. The time-dependent measurement of apoptotic cell death and intracellular ROS using the Incucyte were analyzed using two-way ANOVA and Tukey's multiple comparisons test. Significance was compared to the untreated control for the untransduced A375 and G361 cells. For the transduced cell lines A375-hCYGB and G361-shCYGB statistically significant differences were assessed compared to their respective isogenic control. Unless otherwise noted, qPCR and immunoblotting data were analyzed for statistical significance using one-way ANOVA, followed by Tukey's multiple comparison.

3. Results

3.1. pPBS induces apoptotic cell death in melanoma

The first aim of this study was to assess the anti-tumoral effect of plasma-treated PBS (pPBS) in A375 and G361 melanoma cells. We therefore treated PBS with the kINPen IND for different times and incubated the cells for 24 h before assessing the cell viability and type of cell death. pPBS incubation was able to induce a significant decrease in cell viability in both cell lines, reflecting a pPBS-dependent cytotoxic effect (Fig. 1A and B). Furthermore, longer treatment times of PBS and subsequent incubation resulted in a lower cell viability, indicating a correlation between treatment time and cytotoxicity. Interestingly, A375 cells seemed more sensitive than G361 cells, with responses of both 5 min and 7 min pPBS being significantly different from one another (Fig. S1). Where incubation with 7 min pPBS was able to kill almost all A375 cells after 24 h, cell viability in G361 cells remained 55%.

In addition to overall cell viability, the type of cell death was assessed. Flow cytometric analysis with annexin-V-FITC and PI showed that after 24 h, almost all dead cells were double ($FITC^+/PI^+$) positive, indicative of late-apoptotic cells (Fig. S1). Apoptotic cell death was further validated by an independent assay, where the activation of caspases 3 and 7 was determined (Fig. 1C and D). Caspase 3/7 was clearly activated upon incubation with pPBS. Apoptotic cell death was initiated 8 h after treatment in both cell lines. In the A375, cell death reached a plateau 18 h post treatment, whereas in the G361 cells, no significant increase in (apoptotic) cell death was noticeable after 12 h. Remarkably, incubation with 1 mM NAC before treatment dramatically inhibited caspase 3/7 activity and cell death in both cell lines.

3.2. Intracellular ROS levels are elevated upon pPBS treatment

In a subsequent step, the intracellular ROS levels were measured before and after treatment to verify the mechanism through which pPBS induces its effect. The treatment with pPBS induced a strongly significant and immediate increase in the measured average green fluorescent intensity, both in A375 and G361 cells (Fig. 2C and D). In A375 cells, the measured intensity dropped 6 h after treatment, after which no difference in intracellular ROS between the untreated and pPBS-treated cells was observed. The treatment with 1 mM NAC before pPBS treatment significantly reduced the green fluorescent signal compared to the untreated group, indicating that NAC was able to very efficiently scavenge ROS produced by pPBS.

In G361 cells, the same trend can be observed as that of the A375

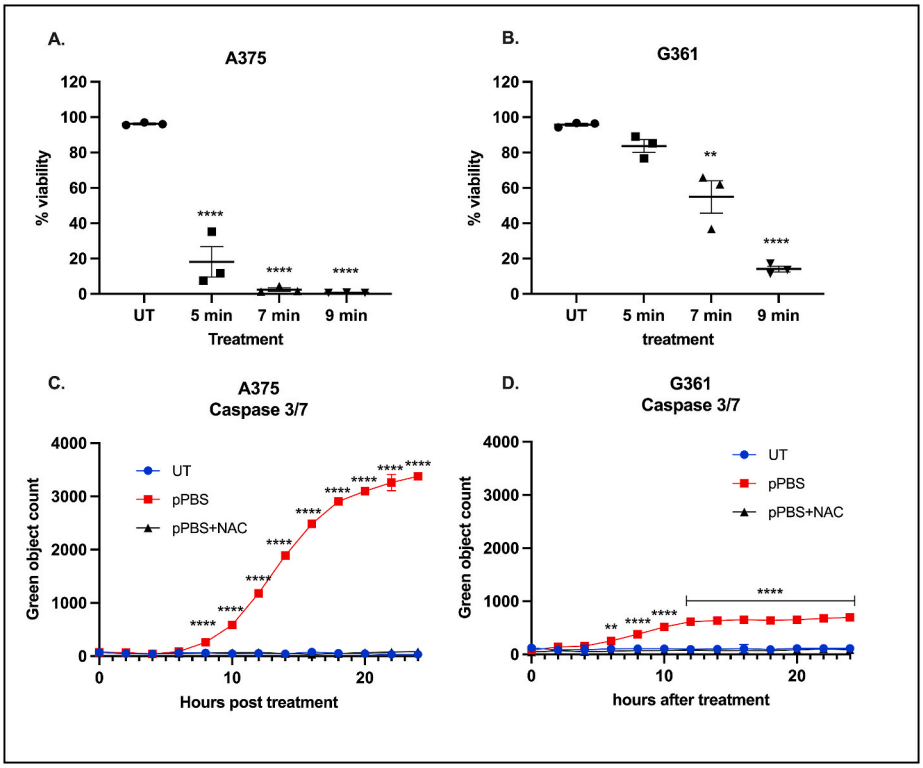

Fig. 1. pPBS induces apoptotic cell death. A375 (A) and G361 (B) cells were treated with 5, 7, or 9 min pPBS, and cell viability was measured 24 h post treatment using flow cytometry. In (C) and (D) apoptotic cell death in respectively A375 and G361 was determined by measuring the activation of caspases 3 and 7 in 2-h intervals for 24 h, using an Incucyte device. A375 and G361 cells were either treated with pPBS only or a combination of 1 mM NAC and pPBS. Results are depicted as the mean with S.E.M of three independent experiments (n = 3). One-way ANOVA (A & B), Two-way ANOVA (C & D) (**$p \leq 0.01$; ****$p \leq 0.0001$). UT, untreated; pPBS, plasma-treated PBS; NAC, *N*-acetyl cysteine.

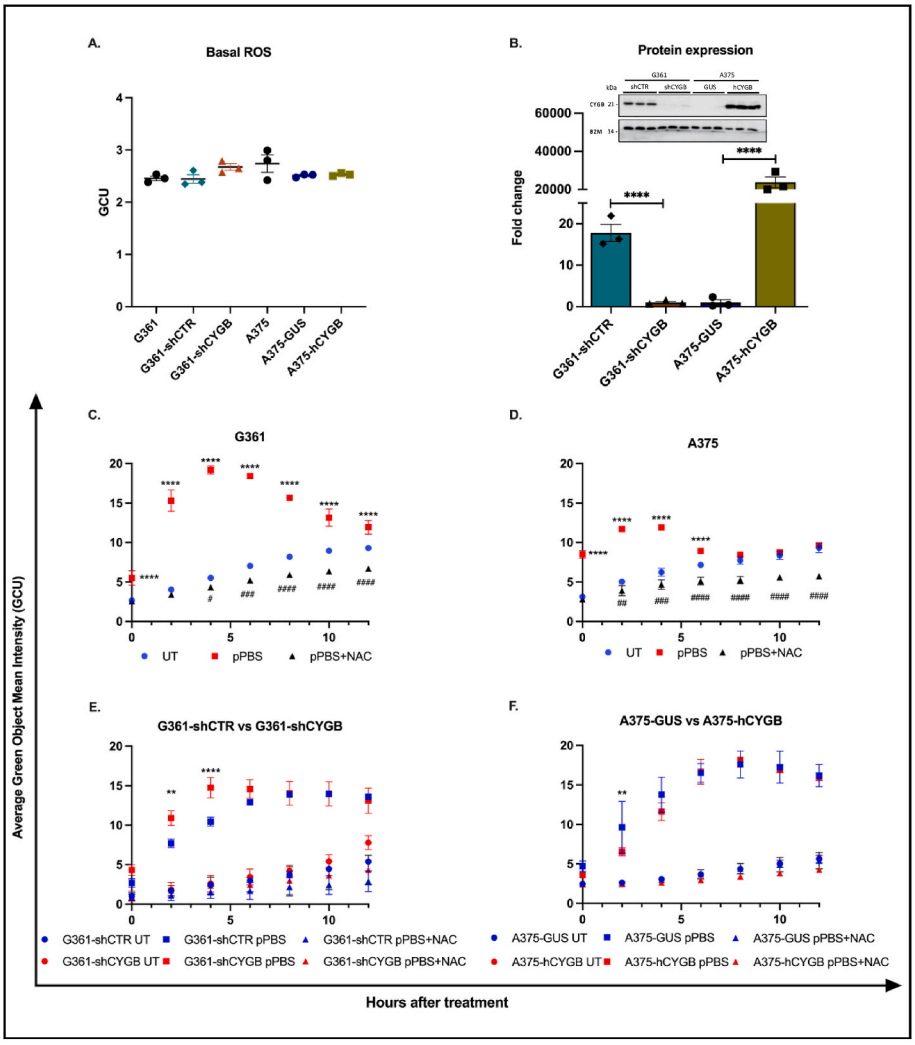

Fig. 2. Intracellular ROS levels are elevated. Intracellular ROS levels were determined with the Incucyte, using the CellROX Green reagent. (A) The basal ROS level of all used cell lines is shown as the average green object mean intensity. (B) Average CYGB protein expression in transduced G361 and A375 cells. G361-shCYGB and A375-hCYGB protein levels were normalized to their respective transgenic controls. B2M was used as loading control. (C) 5min pPBS treatment of A375 cells and (D) 7 min pPBS treatment of G361 cells induced a significant increase in green fluorescent signal compared to the untreated control. (E & F) Intracellular ROS levels of CYGB overexpressing (A375-hCYGB) and CYGB knockdown (G361-shCYGB) cells compared to control cell lines A375-GUS and G361-shCTR. Pre-treatment with 1 mM NAC (pPBS + NAC) significantly reduced intracellular ROS levels compared to the control (mean ± S.E.M; n = 3). Asterisks represent significant difference compared to the respective control cell lines. Two-way ANOVA (**$p \leq 0.01$; ****$p \leq 0.0001$; ##$p \leq 0.01$; ###$p \leq 0.001$; ####$p \leq 0.0001$). UT, untreated; pPBS, plasma-treated PBS; NAC, *N*-acetyl cysteine. (For interpretation of the references to color in this figure legend, the reader is referred to the Web version of this article.)

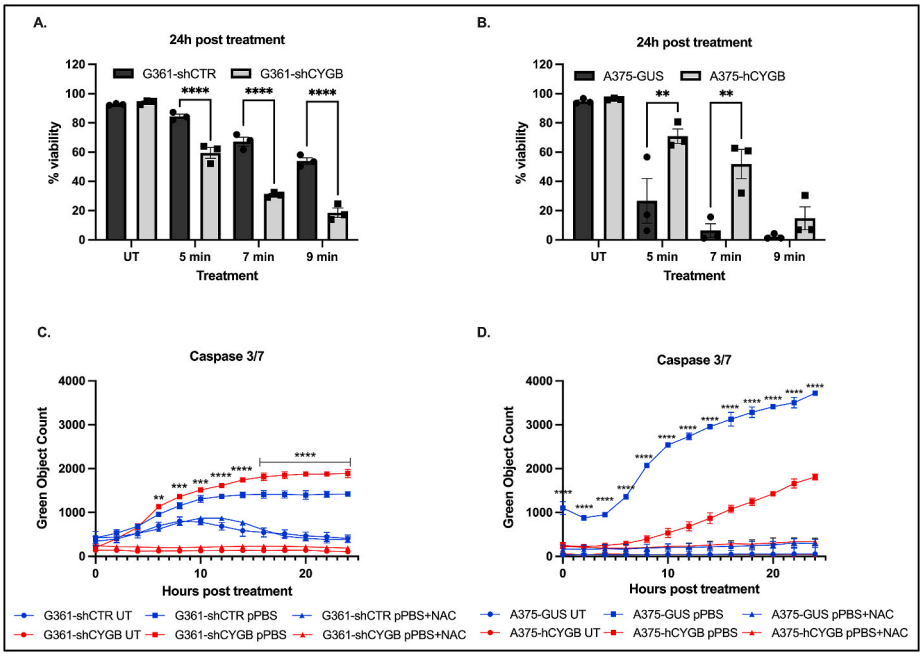

Fig. 3. CYGB protects cells from pPBS treatment. (A) Percentage viable G361-shCTR and G361-shCYGB cells 24 h post treatment. The knockdown of CYGB sensitized G361 cells towards pPBS treatment. (B) Percentage viable A375-GUS and A375-hCYGB cells 24 h after pPBS treatment. CYGB overexpressing A375-hCYGB were more resistant to pPBS treatment. (C) The activation of apoptosis mediators caspase 3/7 in G361-shCTR (blue) was compared to G361-shCYGB (red) during 24 h using an Incucyte device. (D) The amount of apoptotic cell death was determined in A375-GUS (blue) and A375-hCYGB cells (red) (mean ± S.E.M; n = 3). Asterisks represent statistical significance compared to the isogenic control (G361-shCTR or A375-GUS) of the corresponding treatment. Two-way ANOVA (**$p \leq 0.01$; ****$p \leq 0.0001$). UT, untreated; pPBS, plasma-treated PBS; NAC, *N*-acetyl cysteine. (For interpretation of the references to color in this figure legend, the reader is referred to the Web version of this article.)

(Fig. 2C). However, the maximum measured fluorescent signal suggests a higher accumulation of ROS after pPBS treatment compared to A375 cells. Additionally, intracellular ROS levels were still significantly augmented 12 h after treatment. The incubation with NAC prior to pPBS treatment significantly reduced the intracellular ROS content indicating here also that NAC eliminated all pPBS produced ROS. As can be seen in Fig. 2A, no difference in basal ROS levels between A375 and G361 could be observed.

3.3. CYGB overexpression protects, and CYGB knockdown sensitizes cells to pPBS effects

To study the importance of CYGB in determining cell fate after pPBS treatment a CYGB overexpressing A375 cell line (A375-hCYGB) and CYGB knockdown G361 cell line (G361-shCYGB) was established. To account for the possible effect of transduction an A375 cell line overexpressing plant β-glucoronidase (A375-GUS) and a mock-knockdown G361 cell line was also established (G361-shCTR). Immunoblotting illustrated the efficient knockdown of CYGB protein levels. (Fig. 2B).

The knockdown of CYGB in G361 led to a strongly significant decrease in cell viability in all three pPBS treatments compared to the G361-shCTR control cell line (Fig. 3A). In fact, G361-shCTR cell viability 24 h after 9 min pPBS treatment was comparable to the amount of viable G361-shCYGB cells present that were treated with 5 min pPBS. Furthermore, in A375, the overexpression of CYGB greatly protected cells from 5 to 7 min pPBS-induced cell death (Fig. 3B). No significant increase in viable cells could be observed with 9 min pPBS treatment. This data clearly indicates the involvement of CYGB in determining pPBS treatment outcome.

The activation of caspase 3/7 was assessed in a time-dependent manner. Similarly, an increase and decrease in apoptotic cell death can be observed in the CYGB-knockdown G361-shCYGB and CYGB-overexpressing A375-hCYGB, respectively. In G361-shCYGB, a significant increase in caspase 3/7 activation is noticeable from 6 h post treatment onwards (Fig. 3C). In contrast, significantly less caspase 3/7 was activated in A375-hCYGB (Fig. 3D). Incubation with 1 mM NAC before treatment inhibited caspase 3/7 activity and cell death in all cell lines.

Additionally, the intracellular ROS levels were compared between A375-GUS and A375-hCYGB and G361-shCTR and G361-shCYGB (Fig. 2E and F). Initially, significantly higher ROS levels were measured in both A375-GUS and G361-shCYGB compared to their corresponding isogenic control. Although no significant differences were observed in basal ROS levels between cells, a slightly higher signal was measured in the CYGB-knockdown cell line compared to G361-shCTR. In the CYGB-overexpressing cell line a difference is visible between A375 wild-type cells, but not with A375-GUS cells.

3.4. pPBS treatment elicits an antioxidant response on both mRNA and protein level

To investigate the cellular response to pPBS treatment, expression levels of CYGB and two other oxidative stress related genes (HO-1 and NRF2) were measured by qPCR, 6 and 24 h after treatment in the A375-GUS and G361-shCTR cells. In A375-GUS cells, CYGB mRNA levels were significantly downregulated at both 6 and 24 h post treatment (Fig. 4A). Incubation with NAC prior to pPBS treatment also downregulated CYGB mRNA after 6 h but stabilized CYGB expression to baseline after 24 h. Interestingly, in A375-hCYGB cells, CYGB is upregulated more than 2-fold 6 h after treatment, and even 6-fold when pre-incubated with 1 mM NAC (Fig. 4A). The treatment of A375-GUS and hCYGB-overexpressing A375 cells with pPBS induced a steep increase in HO-1 mRNA levels after 6 h, which decreased back to almost baseline after 24 h, or by prior incubation with NAC. There was however a prolonged upregulation noticeable in the CYGB-overexpressing A375 cells, with HO-1 expression levels significantly upregulated in all conditions and timepoints tested (Fig. 4B). Although NRF2 (protein) expression is regulated post-translationally [50], NRF2 mRNA levels were found to be significantly upregulated 6 h after treatment in both A375-GUS and A375-hCYGB and after 24 h in A375-hCYGB only (Fig. 4C).

In G361 control (G361-shCTR) cells CYGB expression remained stable throughout all tested conditions. Remarkably, in the CYGB-knockdown cell line G361-shCYGB, CYGB levels were significantly upregulated 24 h post treatment, even in the presence of 1 mM NAC. The expression pattern of HO-1 in G361-shCTR and G361-shCYGB 6 h after treatment was similar to their respective A375 counterparts (Fig. 4E). Six hours after treatment, HO-1 mRNA levels increased more than 8-fold and 6-fold in G361-shCTR and G361-shCYGB respectively. Although pre-incubation with NAC decreased the effect of pPBS on HO-1 expression after 6 h, HO-1 mRNA was still significantly upregulated. In G361-shCTR, HO-1 levels decreased further to 2-fold the expression of the untreated condition after 24 h. In CYGB-knockdown G361 cells

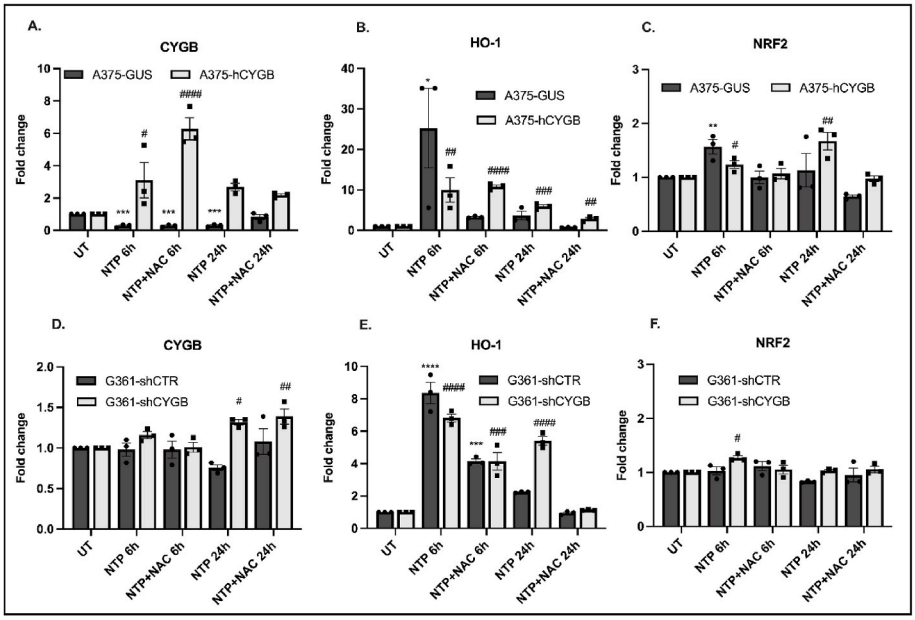

Fig. 4. pPBS treatment induces an antioxidant response at mRNA level. (A–C) Gene expression levels of CYGB, HO-1, and NRF2 in A375-GUS and A375-hCYGB cells. The average fold change mRNA expression of two antioxidant response genes (HO-1 and NRF2) and CYGB, compared to the untreated control (set as 1) was determined 6 and 24 h after pPBS treatment alone, or a combination of 1 mM NAC and pPBS, using qPCR. (D–F) The average fold change gene expression in G361-shCTR and G361-shCYGB cells of two antioxidant response genes (HO-1 and NRF2) and CYGB, compared to the untreated control 6 and 24 h after pPBS treatment alone, or a combination of 1 mM NAC and pPBS. qPCR values were normalized to B2M and YWHAZ (mean ± S.E.M; n = 3). Individual values of replicates are depicted as black dots or squares. One-way ANOVA (**$p \leq 0.01$; ***$p \leq 0.001$; ****$p \leq 0.0001$), ($^{\#}p \leq 0.05$; $^{\#\#}p \leq 0.01$ $^{\#\#\#}p \leq 0.001$; $^{\#\#\#\#}p \leq 0.0001$). UT, untreated; pPBS, plasma-treated PBS; NAC, *N*-acetyl cysteine.

however, HO-1 expression was still significantly upregulated after 24 h. In the NAC pre-treated group, HO-1 expression was not upregulated in both G361 cell lines. Overall, NRF2 expression levels were found to be relatively stable throughout all conditions, with only a statistically significant upregulation found 6 h after pPBS treatment in G361-shCYGB.

Subsequently, the protein expression of CYGB, HO-1, and NRF2 was investigated 6 h after pPBS treatment (Fig. 5A). Immunoblotting analysis showed that pPBS treatment inhibited NRF2 protein degradation, leading to a significant increase in NRF2 protein expression in all tested cell lines except A375-hCYGB, though the latter presented also a non-significant increase in signal (Fig. 5A–E). Interestingly, the pre-incubation of cells with 1 mM NAC induced the same response. This suggests that pPBS exerts the same intracellular effects in these cells, but with different outcomes.

Besides NRF2, HO-1 protein levels were also found to be upregulated 6 h post-treatment. Although the quantification of the immunoblotting signal showed a two-fold upregulation of HO-1 in G361-shCTR, this was not deemed significant. In G361-shCYGB, HO-1 expression was upregulated ~3-fold in both tested conditions (Fig. 5B and C). pPBS treatment of A375-GUS and A375-hCYGB cells significantly induced HO-1 protein after 6 h. However, incubation with NAC prior to treatment, slightly reduced the induction of HO-1 protein after treatment (Fig. 5D and E).

Finally, the quantification of the CYGB immunoblotting signal showed a slight increase in CYGB expression in G361-shCTR cells in pPBS treated cells and a ~2-fold increase in NAC pre-treated cells (Fig. 5B). Interestingly, the CYGB-knockdown cell line G361-shCYGB also displayed a significant upregulation of CYGB expression in both tested conditions (Fig. 5C). Although in A375-GUS cells CYGB expression appeared to be significantly upregulated, the measured signal was acquired after extensive exposure, as A375-GUS expresses almost no endogenous CYGB (Fig. 6A). In the CYGB-overexpressing cell line A375-hCYGB, no significant upregulation was found 6 h after pPBS treatment. However, a slight, yet significant increase in CYGB expression could be observed in the NAC pre-treated group (Fig. 5E).

3.5. The presence of CYGB affects HO-1 and NRF2 expression

As the overexpression and/or knockdown of CYGB could potentially affect the basal cellular state, we compared the basal protein (and mRNA; see Fig. S3) levels of NRF2, HO-1 and CYGB between cells. Immunoblotting showed that the used overexpressing and knockdown systems of CYGB were very efficient (Fig. 6A, C, and D). Although CYGB mRNA expression was very similar in G361-shCTR and A375-hCYGB (Fig. S2), CYGB protein levels were clearly superior in A375-hCYGB. A substantial difference in basal expression levels of NRF2, CYGB and HO-1 was observed between G361-shCTR and A375-GUS (Fig. 6B). When comparing the protein levels of CYGB, HO-1, and NRF2 between G361-shCTR and G361-shCYGB, a significantly higher expression of all three proteins can be observed in G361-shCTR. Furthermore, the knockdown of CYGB resulted in a 2-fold decrease in HO-1 and NRF2 (Fig. 6A and D). In contrast, A375-hCYGB exhibited a strongly significant increase (besides CYGB) in HO-1 and NRF2 (Fig. 6C). Thus, it seems that the presence of CYGB enhances HO-1 and NRF2 expression levels, whereas the absence impairs their expression.

3.6. Transcriptomics reveal differentially expressed genes in G361-shCYGB

To explore the CYGB-dependent transcriptome we performed RNA-seq on G361-shCTR and G361-shCYGB cells under basal conditions. Three independent samples for each genotype were analyzed and the

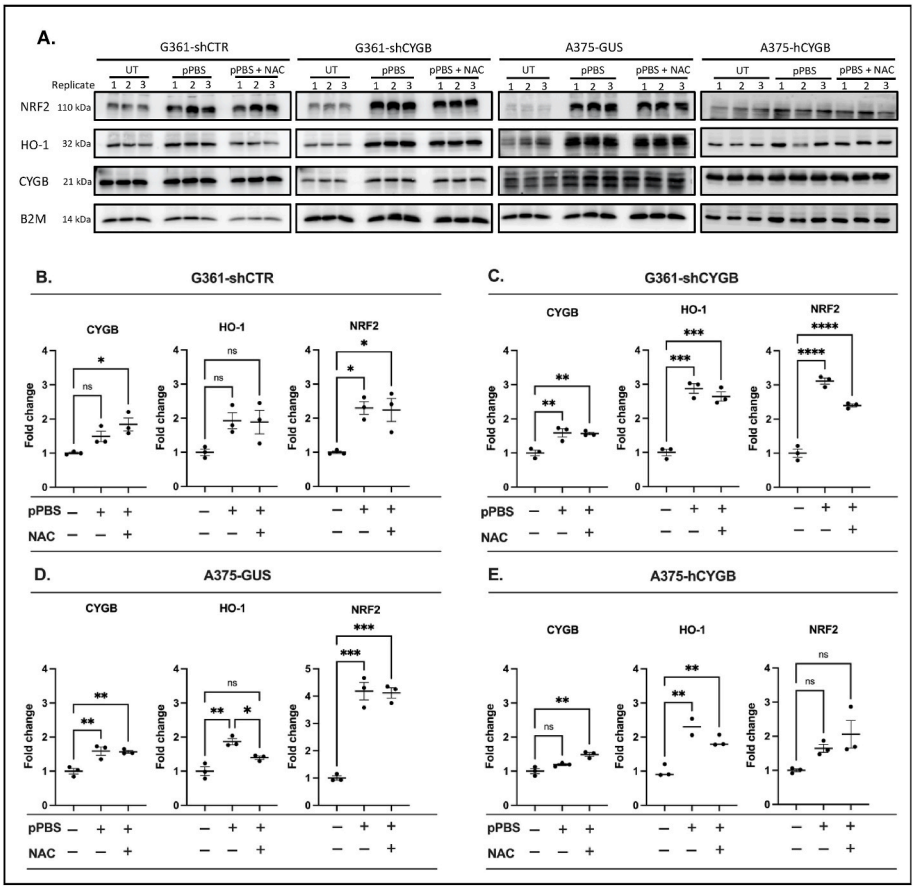

Fig. 5. Protein expression of HO-1, NRF2 and CYGB is upregulated. (A) Immunoblots of G361-shCTR, G361-shCYGB, A375-GUS, and A375-hCYGB showing 3 biological replicates of untreated, pPBS only (pPBS), or pre-treated with 1 mM NAC (NAC) cells, 6 h post treatment. HO-1, NRF2, and CYGB were revealed using their respective rabbit polyclonal antibodies. B2M was used as loading control. (B–E) The average fold change protein expression of HO-1, NRF2, and CYGB in G361-shCTR (B), G361-shCYGB (C), A375-GUS (D), A375-hCYGB (E), compared to the untreated control (set as 1). Quantified immunoblot signals were normalized to the loading control B2M (mean ± S.E.M; n = 3). Individual values of replicates are depicted as black dots. One-way ANOVA (**p ≤ 0.01; ***p ≤ 0.001; ****p ≤ 0.0001). pPBS, plasma-treated PBS; NAC, *N*-acetyl cysteine.

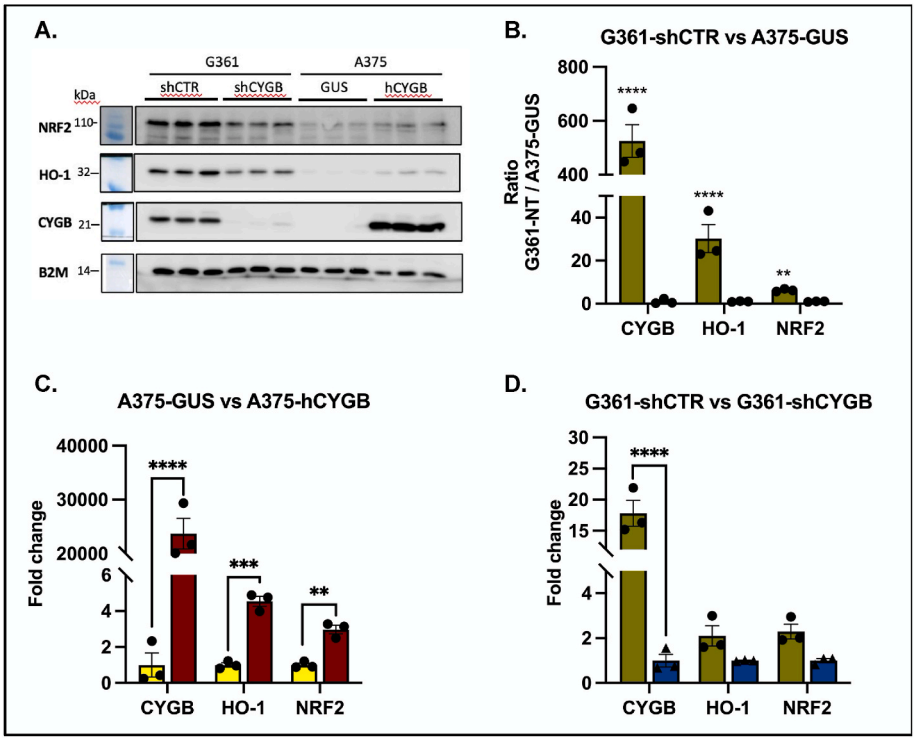

Fig. 6. CYGB affects HO-1 and NRF2 expression. (A) Immunoblots of untreated G361-shCTR, G361-shCYGB, A375-GUS, and A375-hCYGB showing 3 biological replicates. HO-1, NRF2, and CYGB were revealed using their respective rabbit polyclonal antibodies. B2M was used as loading control. (B) The ratio of the average protein expression of G361-shCTR versus A375-GUS (set as 1) to compare differences in basal expression of HO-1, NRF2, and CYGB. (C) The average fold change difference in expression between A375-hCYGB (CYGB-overexpressing) and A375-GUS (set as 1) of each probed protein. (D) The average fold change difference in protein expression of G361-shCTR compared to the CYGB-knockdown cell line (G361-shCYGB). Quantified immunoblot signals were normalized to the loading control B2M (mean ± S.E.M; n = 3). Individual values of replicates are depicted as black dots. Two-way ANOVA (**p ≤ 0.01; ***p ≤ 0.001; ****p ≤ 0.0001).

knockdown efficiency of shCYGB was confirmed to be >90%. Differential analysis of normalized counts using DESeq2 identified 316 genes that were differentially expressed. Of those 316 genes, 111 genes (26 up- and 85 downregulated) were differentially expressed above an absolute $\log_2$ fold change of 1 (DEGs; Fig. 7A). One of the top DEGs identified was the long non-coding RNA (lncRNA) maternally expressed gene 3 (MEG3). MEG3 expression was dramatically downregulated in CYGB knockdown G361-shCYGB compared to G361-shCTR cells. Additionally, the observed downregulation of MEG3 in G361-shCYGB cells was validated in an independent qPCR experiment (Fig. 7B). Hence, the presence

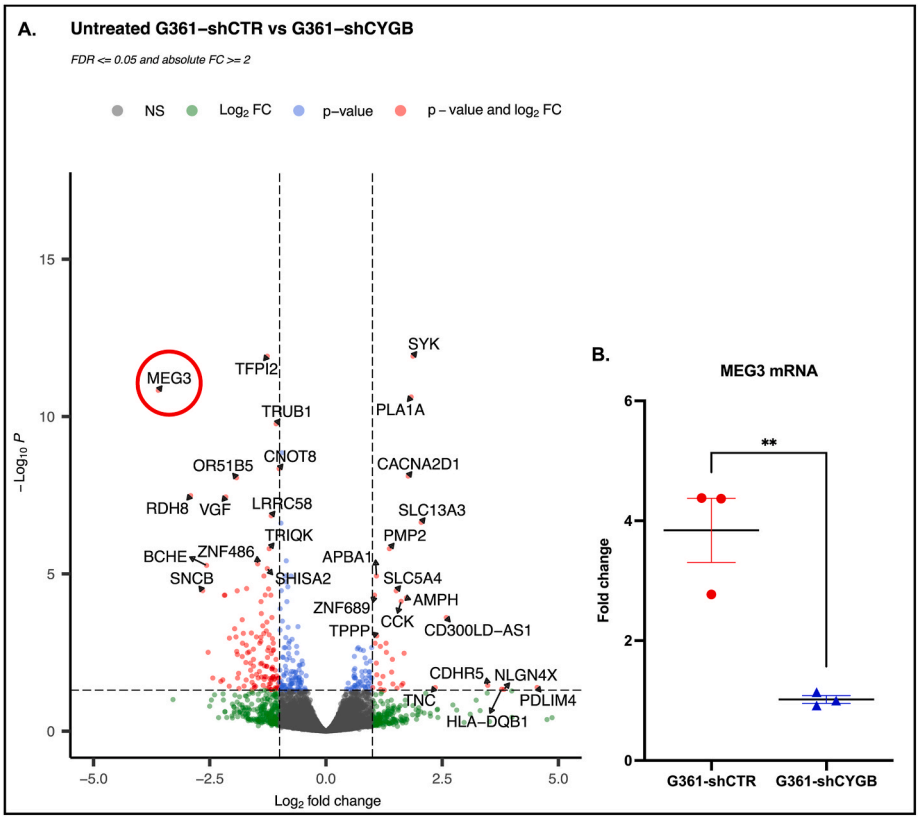

Fig. 7. Basal CYGB-dependent transcriptome. Comparison of the G361-shCTR and G361-shCYGB transcriptomes under basal conditions. (A) Enhanced volcano plot plots the differentially expressed genes based on their Log_2 fold change (Log_2FC) and -Log_{10} p-adjusted value (-Log_{10} *P*). CYGB was excluded from plotting. Individual genes were color coded depending on the set Log_2FC and (-Log_{10} *P*) thresholds. (B) Fold change mRNA expression compared to G361-shCYGB cell line (set as 1). Relative quantities were normalized to B2M and YWHAZ (mean ± S.E.M; n = 3). Individual values of replicates are depicted as red dots or blue triangles. Student's t-test (**p ≤ 0.01). (For interpretation of the references to color in this figure legend, the reader is referred to the Web version of this article.)

or absence of CYGB seems to influence the expression of lncRNA MEG3.

4. Discussion

In this study, the sensitivity of two different melanoma cell lines, expressing different levels of endogenous CYGB, towards pPBS treatment was investigated. The NTP treatment of PBS induced an exposure time-dependent reduction in cell viability in both A375 and G361 cell lines, demonstrating the cytotoxicity of NTP-treated liquids (Fig. 1A and B). Additionally, pPBS treatment mainly induced cell death through apoptosis, as shown by the activation of caspases 3 and 7 (Fig. 1C and D) and annexin V-FITC/PI staining (Fig. S1). The mediators of the cytotoxicity of NTP have previously been shown to be attributed to the production of multiple short-lived and long-lived RONS [51,52]. In NTP-treated solutions, however, long-lived RONS like H_2O_2, NO_2^- and NO_3^- are considered the main effectors of the cytotoxic and genotoxic effects observed in cancer cells [44,45].

Indeed, here we found that incubation with pPBS induced a rapid elevation of intracellular ROS levels and that the pre-incubation with NAC could abrogate this response (Fig. 2B and C). NAC is a synthetic precursor of intracellular cysteine and glutathione, and its antioxidant activity results from its free radical scavenging properties, either directly via the redox potential of thiols or secondarily via increasing glutathione (GSH) levels in the cells [53]. The treatment with NAC increased GSH levels consistently in all employed cell models (Fig. S5). Therefore, the incubation with NAC prior to pPBS treatment boosts the cellular antioxidant defense systems, thereby dramatically reducing the accumulation of ROS and ROS-induced apoptosis (Figs. 1 and 2). Collectively our findings are consistent with previous studies supporting that pPBS cytotoxicity is mediated through the production of RO(N)S and leads to apoptotic cell death [45].

As the pre-incubation with NAC showed, cellular antioxidant mechanisms are in place to protect cells from the detrimental effects of increased levels of RONS, also known as oxidative stress. NRF2 is a transcription factor responsible for the regulation of cellular redox balance and protective antioxidant and phase II detoxification responses in mammals [54]. NRF2 controls the expression of key components of the glutathione and thioredoxin antioxidant system, as well as enzymes involved in NADPH regeneration, ROS and xenobiotic detoxification, and heme metabolism, thus playing a fundamental role in maintaining the redox homeostasis of the cell [55]. Here, we showed that pPBS treatment induced NRF2 protein expression in A375 and G361 cells (Fig. 5), but mRNA expression remained largely unchanged (Fig. 4C and F), with only a significant upregulation in NRF2 mRNA found in A375 cells 6 h after treatment. Previous studies have shown that NRF2 activity and abundance are tightly regulated at the transcriptional, post-transcriptional, and post-translational level [50,56,57]. Therefore, the observed upregulation in A375 cells is most likely of no biological importance. One of the genes regulated through NRF2 is HO-1 [58]. Besides NRF2, HO-1 is strongly upregulated by several stimuli, including heme, nitric oxide, heavy metals, growth factor, cytokines, and modified lipids. Here, we demonstrated that HO-1 mRNA and protein expression was highly upregulated in A375 and G361 cells after pPBS treatment (Fig. 4B and D).

Interestingly, cells that were pre-treated with NAC also showed an increase in NRF2 (and to a lesser extent, HO-1) protein levels. This would imply that NRF2 is activated by pPBS-induced ROS but that NAC aids in the protection of the cell. However, no increase in intracellular ROS upon pPBS administration was observed in cells pre-treated with NAC. Yet, pPBS treatment caused a drop in GSH levels in cells pre-treated with NAC (Fig. S5). This suggests that ROS were present in NAC pre-treated cells upon pPBS treatment but were efficiently neutralized by the increased levels of GSH. Considering that GSH also serves as a substrate or cofactor of many NRF2-regulated detoxifying cellular enzymes [59], and NRF2 is critical for maintaining the GSH redox state via transcriptional regulation of glutathione reductase [60], it is likely that NAC (through increasing the total GSH content) contributed to the induction of NRF2 (and HO-1) protein levels.

The aforementioned findings on the molecular and cellular responses to pPBS treatment were very similar in both A375 and G361 cells. However, A375 cells were much more sensitive to pPBS treatment compared to G361. This suggests possible cell type specific differences in the ability to eliminate the RONS produced by pPBS treatment. As A375 cells display low endogenous CYGB levels, while G361 cells display rather high levels, we investigated the potential involvement of CYGB in determining the sensitivity to pPBS by establishing a CYGB-overexpressing A375 cell line (A375-hCYGB) and a CYGB-knockdown G361 cell line (G361-shCYGB) together with their corresponding isogenic controls (i.e., A375-GUS and G361-shCTR). Overexpression of CYGB in A375-hCYGB and knockdown in G361-shCYGB respectively rescued and sensitized cells to pPBS treatment. Furthermore, significantly less cells underwent programmed cell death through apoptosis (Fig. 3). Although no significant difference in basal intracellular ROS was found between A375-hCYGB, G361-shCYGB, and their respective controls (Fig. 2A), the overexpression of CYGB slightly (but significantly) reduced the intracellular ROS content after pPBS treatment, and increased ROS levels in CYGB knockdown cells. Thus, it seems that CYGB expression protects melanoma cells from ROS-induced apoptosis by the scavenging of ROS. However, a direct ROS scavenging function is unlikely, as previous biochemical studies have shown the reaction rate of CYGB with H_2O_2 to be several orders of magnitude slower than specialized metal- and thiol-based peroxidases [22]. In contrast, a nitric oxide dioxygenase and nitrite reductase activity has received experimental support [61–63]. As NTP-treated solutions like pPBS also contain nitrogen species, CYGB could aid cell survival after pPBS treatment by detoxifying RNS.

We cannot exclude that the cytoprotective effect of CYGB occurs independent from direct antioxidant properties. In fact, here we found the protein expression of NRF2 and HO-1 to be dysregulated upon CYGB knockdown and overexpression (Fig. 6). This was especially noticeable in CYGB-overexpressing A375-hCYGB. The reason why this effect was greater in A375-hCYGB might be explained by the much larger (relative) change in CYGB expression. Yet, in G361-shCYGB cells, NRF2 and HO-1 levels were reduced by half, which could potentially have a large biological impact. This is in accordance with other studies that showed a downregulation of antioxidant enzymes or a dysregulation of the NRF2 pathway upon loss of CYGB [24,64–66].

NRF2s involvement in heme biosynthesis could possibly explain these findings [67]. Several genes involved in the heme biosynthetic pathway are transcriptional targets of NRF2. Thus, it is possible that the high levels of endogenous CYGB in G361-shCTR demand a higher level of basal NRF2 to maintain adequate levels of heme biosynthesis. At the same time, the excessive production of heme could either directly itself induce HO-1 protein levels, or indirectly through NRF2 activation [68].

Interestingly, a possible mechanism through which CYGB can regulate NRF2 and HO-1 expression is represented by the lncRNA MEG3. MEG3 was one of the DEGs identified to be dramatically downregulated in G361-shCYGB cells (Fig. 7). Strong evidence exists that MEG3 is a lncRNA tumor suppressor [69]. One way MEG3 can exert its tumor-suppressive function is by acting as a competing endogenous RNA (ceRNA) for shared microRNAs (miRNAs) [70]. miRNAs involvement in the post-transcriptional regulation of NRF2 has been demonstrated in multiple studies [71–73]. MEG3 has been shown to regulate NRF2 expression in hepatocytes and retinal pigment endothelial cells by acting as a ceRNA for miRNAs targeting NRF2. Moreover, RNA immunoprecipitation analysis revealed MEG3-NRF2 protein formation in fibroblasts, which positively affected NRF2 protein levels [74]. In melanoma, MEG3 expression suppressed melanoma development, growth, and metastasis through modulation of several cancer-associated pathways [75–77]. It is therefore conceivable that CYGB can regulate NRF2 and its downstream target HO-1 through the regulation of MEG3 lncRNA levels. Additionally, the correlation between CYGB and MEG3 expression sheds

a new light on the tumor-suppressive function of CYGB. Notably, the expression levels of MEG3 are nearly undetectable in the endogenously low CYGB expressing A375 cell line [76], which was also found in this study (data not shown). However, CYGB overexpression did not increase MEG3 expression.

Furthermore, CYGB mRNA expression was found to be upregulated upon pPBS treatment in A375-hCYGB and G361-shCYGB, and CYGB protein levels in all cells. Recently, chromatin immunoprecipitation analysis of the human regulatory region of CYGB identified the transcription factor p63 as an important transcriptional regulator of cytoglobin expression in keratinocytes via direct binding to the *CYGB* promoter [78]. The ΔNp63 isoform targets multiple genes involved in the oxidative stress response [79,80]. Hence, the pPBS treatment-dependent regulation of CYGB was possibly mediated by ΔNp63. In addition, NRF2 was shown to bind to the promiscuous activator protein 1 (AP-1) binding site of β-globin [81]. As an AP-1 response element has been located within the upstream region of the CYGB gene [82], the observed induction of CYGB mRNA and protein could, at least partly, be explained by NRF2-mediated activation of the CYGB promoter. We should note however that CYGB expression in A375-hCYGB is under the control of a cytomegalovirus (CMV) promoter. Thus, CYGB mRNA and protein induction upon pPBS treatment in CYGB overexpressing A375-hCYGB cells is likely of no biological importance. The CMV promoter has been shown to be induced upon cellular stresses, including oxidative stress [83,84].

Previously, we showed that NTP-produced RONS lead to the formation of an intramolecular disulfide bridge that would allow CYGB to function as a redox-sensitive protein [21]. Therefore, we believe it is plausible that CYGB protects cells from pPBS cytotoxicity first by maintaining a higher basal antioxidant defense via upregulating the master regulator NRF2 (and downstream targets), and second by aiding in the detoxification of RONS via acting as a redox-sensitive switch in an antioxidant response signaling cascade.

Thus, the presence of CYGB, at least in melanoma cells, seems to play a central role in determining the therapeutic outcome of ROS-inducing anticancer therapies, like NTP-treated solutions. Furthermore, the presence of CYGB influenced MEG3 expression (and subsequently NRF2) in G361 cells, which warrants further investigation into the interplay between CYGB and MEG3. CYGB expression is frequently downregulated (through hypermethylation) in melanocyte-to-melanoma transition, which would suit a tumor-suppressive role. However, in melanoma cells that still abundantly express CYGB, its function could also be seen as rather oncogenic, especially under stress conditions. Hence, CYGB expression could be of interest either as a biomarker or as a candidate for future targeted therapies in melanoma.

5. Conclusion

Taken together, our data showed that pPBS treatment leads to apoptotic cell death in melanoma cells through the production of ROS, and that the presence of CYGB plays a key role in determining the outcome of ROS-based anticancer therapies. Furthermore, pPBS treatment elicited an NRF2-mediated antioxidant response. The expression of CYGB was upregulated upon pPBS treatment and CYGB expression itself positively regulated NRF2 and HO-1 protein levels. CYGB possibly exerts its cytoprotective effect indirectly by serving as a redox-sensitive protein. Moreover, transcriptomics revealed aberrant expression of the tumor suppressor MEG3 upon CYGB knockdown, which proposes a novel mechanism for CYGBs role as a tumor suppressor and cytoprotective protein. As CYGB expression is frequently downregulated (through hypermethylation) in melanocyte-to-melanoma transition, CYGB expression could be of interest either as a biomarker or as a candidate for future targeted therapies in melanoma.

Declaration of competing interest

The authors declare that they have no known competing financial interests or personal relationships that could have appeared to influence the work reported in this paper.

Acknowledgments

This work was funded in part by the Research Foundation - Flanders (FWO) and the Flemish Government. The FWO fellowships and grants that funded this work include: 12S9221 N (Abraham Lin) and G044420 N (Abraham Lin and Annemie Bogaerts). Joey De Backer acknowledges a visiting fellowship from the University of Fribourg. David Hoogewijs acknowledges support by the Swiss National Science Foundation (grants 31003A_173000 and 310030_207460).

Appendix A. Supplementary data

Supplementary data to this article can be found online at https://doi.org/10.1016/j.redox.2022.102399.

References

[1] R.L. Siegel, K.D. Miller, A. Jemal, Cancer statistics, 2020, CA A Cancer J. Clin. 70 (1) (2020) 7–30.
[2] X. Sun, et al., Ultraviolet radiation and melanomagenesis: from mechanism to immunotherapy, Front. Oncol. 10 (2020), 951-951.
[3] Anna, B., et al., Mechanism of UV-Related Carcinogenesis and its Contribution to Nevi/melanoma. (1746-9872 (Print)).
[4] Y. Kim, Y.-Y. He, Ultraviolet radiation-induced non-melanoma skin cancer: regulation of DNA damage repair and inflammation, Gene Dis. 1 (2) (2014) 188–198.
[5] E. Kvam, R.M. Tyrrell, Induction of oxidative DNA base damage in human skin cells by UV and near visible radiation, Carcinogenesis 18 (12) (1997) 2379–2384.
[6] M. Cichorek, et al., Skin melanocytes: biology and development, Postepy Dermatol. Alergol. 30 (1) (2013) 30–41.
[7] N. Kobayashi, et al., Supranuclear melanin caps reduce ultraviolet induced DNA photoproducts in human epidermis, J. Invest. Dermatol. 110 (5) (1998) 806–810.
[8] A.L. Kadekaro, et al., alpha-Melanocortin and endothelin-1 activate antiapoptotic pathways and reduce DNA damage in human melanocytes, Cancer Res. 65 (10) (2005) 4292–4299.
[9] J.D. Simon, et al., Current challenges in understanding melanogenesis: bridging chemistry, biological control, morphology, and function, Pigm. Cell. Melanoma Res. 22 (5) (2009) 563–579.
[10] L. Denat, et al., Melanocytes as instigators and victims of oxidative stress, J. Invest. Dermatol. 134 (6) (2014) 1512–1518.
[11] Y. Liu, et al., Comparison of structural and chemical properties of black and red human hair melanosomes, Photochem. Photobiol. 81 (1) (2005) 135–144.
[12] P. Di Donato, A. Napolitano, G. Prota, Metal ions as potential regulatory factors in the biosynthesis of red hair pigments: a new benzothiazole intermediate in the iron or copper assisted oxidation of 5-S-cysteinyldopa, Biochim. Biophys. Acta 1571 (2) (2002) 157–166.
[13] N.C. Jenkins, et al., The p16(INK4A) tumor suppressor regulates cellular oxidative stress, Oncogene 30 (3) (2011) 265–274.
[14] P.B. Cassidy, et al., Selenium for the prevention of cutaneous melanoma, Nutrients 5 (3) (2013) 725–749.
[15] B. Govindarajan, et al., Overexpression of Akt converts radial growth melanoma to vertical growth melanoma, J. Clin. Invest. 117 (3) (2007) 719–729.
[16] S.R. Pinnell, Cutaneous photodamage, oxidative stress, and topical antioxidant protection, J. Am. Acad. Dermatol. 48 (1) (2003) 1–19. ; quiz 20-2.
[17] A. Kokot, et al., Alpha-melanocyte-stimulating hormone counteracts the suppressive effect of UVB on Nrf2 and Nrf-dependent gene expression in human skin, Endocrinology 150 (7) (2009) 3197–3206.
[18] A.L. Kadekaro, et al., Melanocortin 1 receptor genotype: an important determinant of the damage response of melanocytes to ultraviolet radiation, Faseb. J. 24 (10) (2010) 3850–3860.
[19] C. Diehl, Melanocytes and oxidative stress, J. Pigmentary Disord. 1 (2014).
[20] Y. Fujita, et al., Melanoma transition is frequently accompanied by a loss of cytoglobin expression in melanocytes: a novel expression site of cytoglobin, PLoS One 9 (4) (2014), e94772.
[21] J. De Backer, et al., The effect of reactive oxygen and nitrogen species on the structure of cytoglobin: a potential tumor suppressor, Redox Biol. 19 (2018) 1–10.
[22] C. Mathai, et al., Emerging perspectives on cytoglobin, beyond NO dioxygenase and peroxidase, Redox Biol. 32 (2020), 101468.
[23] A. Keppner, et al., Lessons from the post-genomic era: globin diversity beyond oxygen binding and transport, Redox Biol. 37 (2020), 101687.
[24] E.B. Randi, et al., The antioxidative role of cytoglobin in podocytes: implications for a role in chronic kidney Disease, Antioxidants Redox Signal. 32 (16) (2020) 1155–1171.

[25] J.L. Zweier, et al., Cytoglobin has potent superoxide dismutase function, Proc. Natl. Acad. Sci. USA 118 (52) (2021) e2105053118.
[26] E. Stoffels, et al., Plasma needle forin vivomedical treatment: recent developments and perspectives, Plasma Sources Sci. Technol. 15 (4) (2006) S169–S180.
[27] G.J. Kim, et al., DNA damage and mitochondria dysfunction in cell apoptosis induced by nonthermal air plasma, Appl. Phys. Lett. 96 (2) (2010), 021502.
[28] E. Stoffels, Y. Sakiyama, D.B. Graves, Cold atmospheric plasma: charged species and their interactions with cells and tissues, IEEE Trans. Plasma Sci. 36 (4) (2008) 1441–1457.
[29] D. Yan, J.H. Sherman, M. Keidar, Cold atmospheric plasma, a novel promising anti-cancer treatment modality, Oncotarget 8 (9) (2017) 15977–15995.
[30] K.D. Weltmann, T. von Woedtke, Plasma medicine—current state of research and medical application, Plasma Phys. Contr. Fusion 59 (1) (2016), 014031.
[31] X. Lu, et al., Reactive species in non-equilibrium atmospheric-pressure plasmas: generation, transport, and biological effects, Phys. Rep. 630 (2016) 1–84.
[32] D.B. Graves, Reactive species from cold atmospheric plasma: implications for cancer therapy, Plasma Process. Polym. 11 (12) (2014) 1120–1127.
[33] R. Furuta, et al., Intracellular responses to reactive oxygen and nitrogen species, and lipid peroxidation in apoptotic cells cultivated in plasma-activated medium, Plasma Process. Polym. 14 (11) (2017), 1700123.
[34] A.M. Hirst, et al., Low-temperature plasma treatment induces DNA damage leading to necrotic cell death in primary prostate epithelial cells, Br. J. Cancer 112 (9) (2015) 1536–1545.
[35] A. Privat-Maldonado, et al., Reduction of human glioblastoma spheroids using cold atmospheric plasma: the combined effect of short- and long-lived reactive species, Cancers 10 (11) (2018).
[36] J. Hou, et al., Non-thermal plasma treatment altered gene expression profiling in non-small-cell lung cancer A549 cells, BMC Genom. 16 (1) (2015) 435.
[37] A. Lin, et al., Non-thermal plasma as a unique delivery system of short-lived reactive oxygen and nitrogen species for immunogenic cell death in melanoma cells, Adv. Sci. 6 (6) (2019), 1802062.
[38] S. Bekeschus, Combined toxicity of gas plasma treatment and nanoparticles exposure in melanoma cells in vitro, Nanomaterials (Basel) 11 (3) (2021).
[39] K.R. Liedtke, et al., Non-thermal plasma-treated solution demonstrates antitumor activity against pancreatic cancer cells in vitro and in vivo, Sci. Rep. 7 (1) (2017) 8319.
[40] H. Tanaka, et al., Similarities and differences in the cellular resposnses between plasma-activated medium-treated glioblastomas and plasma-activated ringer's lactate solution-treated glioblastomas, Clin. Plasma Med. 9 (2018) 42–43.
[41] A. Schörg, et al., Destruction of a distal hypoxia response element abolishes trans-activation of the PAG1 gene mediated by HIF-independent chromatin looping, Nucleic Acids Res. 43 (12) (2015) 5810–5823.
[42] T.W. Koay, et al., Androglobin gene expression patterns and FOXJ1-dependent regulation indicate its functional association with ciliogenesis, J. Biol. Chem. 296 (2021), 100291.
[43] S. Reuter, T. von Woedtke, K.-D. Weltmann, The kINPen—a review on physics and chemistry of the atmospheric pressure plasma jet and its applications, J. Phys. Appl. Phys. 51 (23) (2018), 233001.
[44] E. Griseti, N. Merbahi, M. Golzio, Anti-cancer potential of two plasma-activated liquids: implication of long-lived reactive oxygen and nitrogen species, Cancers 12 (3) (2020).
[45] H. Tanaka, et al., Plasma-treated solutions (PTS) in cancer therapy, Cancers 13 (7) (2021) 1737.
[46] J. De Backer, et al., A reliable set of reference genes to normalize oxygen-dependent cytoglobin gene expression levels in melanoma, Sci. Rep. 11 (1) (2021), 10879.
[47] J.H. Fuady, et al., Hypoxia-inducible factor-mediated induction of WISP-2 contributes to attenuated progression of breast cancer, Hypoxia (Auckl) 2 (2014) 23–33.
[48] A. Keppner, et al., Deletion of the serine protease CAP2/Tmprss4 leads to dysregulated renal water handling upon dietary potassium depletion, Sci. Rep. 9 (1) (2019), 19540.
[49] M.I. Love, W. Huber, S. Anders, Moderated estimation of fold change and dispersion for RNA-seq data with DESeq2, Genome Biol. 15 (12) (2014) 550.
[50] J.D. Hayes, A.T. Dinkova-Kostova, The Nrf2 regulatory network provides an interface between redox and intermediary metabolism, Trends Biochem. Sci. 39 (4) (2014) 199–218.
[51] A. Lin, et al., Oxidation of innate immune checkpoint CD47 on cancer cells with non-thermal plasma, Cancers 13 (3) (2021) 579.
[52] A. Lin, et al., Nanosecond-pulsed DBD plasma-generated reactive oxygen species trigger immunogenic cell death in A549 lung carcinoma cells through intracellular oxidative stress, Int. J. Mol. Sci. 18 (5) (2017) 966.
[53] S.-Y. Sun, N-acetylcysteine, reactive oxygen species and beyond, Cancer Biol. Ther. 9 (2) (2010) 109–110.
[54] A. Loboda, et al., Role of Nrf2/HO-1 system in development, oxidative stress response and diseases: an evolutionarily conserved mechanism, Cell. Mol. Life Sci. 73 (17) (2016) 3221–3247.
[55] C. Gorrini, I.S. Harris, T.W. Mak, Modulation of oxidative stress as an anticancer strategy, Nat. Rev. Drug Discov. 12 (12) (2013) 931–947.
[56] D. Stewart, et al., Degradation of transcription factor Nrf2 via the ubiquitin-proteasome pathway and stabilization by cadmium, J. Biol. Chem. 278 (4) (2003) 2396–2402.
[57] T. Nguyen, et al., Increased protein stability as a mechanism that enhances Nrf2-mediated transcriptional activation of the antioxidant response element. Degradation of Nrf2 by the 26 S proteasome, J. Biol. Chem. 278 (7) (2003) 4536–4541.
[58] J. Alam, et al., Nrf2, a Cap'n'Collar transcription factor, regulates induction of the heme oxygenase-1 gene, J. Biol. Chem. 274 (37) (1999) 26071–26078.
[59] V.I. Lushchak, Glutathione Homeostasis and Functions: Potential Targets for Medical Interventions, vol. 2012, J Amino Acids, 2012, 736837.
[60] C.J. Harvey, et al., Nrf2-regulated glutathione recycling independent of biosynthesis is critical for cell survival during oxidative stress, Free Radic. Biol. Med. 46 (4) (2009) 443–453.
[61] X. Liu, et al., Characterization of the function of cytoglobin as an oxygen-dependent regulator of nitric oxide concentration, Biochemistry 51 (25) (2012) 5072–5082.
[62] J.L. Zweier, G. Ilangovan, Regulation of nitric oxide metabolism and vascular tone by cytoglobin, Antioxidants Redox Signal. 32 (16) (2020) 1172–1187.
[63] B.J. Reeder, J. Ukeri, Strong modulation of nitrite reductase activity of cytoglobin by disulfide bond oxidation: implications for nitric oxide homeostasis, Nitric Oxide 72 (2018) 16–23.
[64] S. Zhang, et al., Cytoglobin promotes cardiac progenitor cell survival against oxidative stress via the upregulation of the NFκB/iNOS signal pathway and nitric oxide production, Sci. Rep. 7 (1) (2017), 10754.
[65] S. Singh, et al., Cytoglobin modulates myogenic progenitor cell viability and muscle regeneration, Proc. Natl. Acad. Sci. U. S. A. 111 (1) (2014) E129–E138.
[66] L.S. Thorne, et al., Cytoglobin protects cancer cells from apoptosis by regulation of mitochondrial cardiolipin, Sci. Rep. 11 (1) (2021) 985.
[67] M.J. Kerins, A. Ooi, The roles of NRF2 in modulating cellular iron homeostasis, Antioxidants Redox Signal. 29 (17) (2018) 1756–1773.
[68] S.K. Chiang, S.E. Chen, L.C. Chang, A dual role of heme oxygenase-1 in cancer cells, Int. J. Mol. Sci. 20 (1) (2018).
[69] Y. Zhou, X. Zhang, A. Klibanski, MEG3 noncoding RNA: a tumor suppressor, J. Mol. Endocrinol. 48 (3) (2012) R45–R53.
[70] S. Bhattacharjee, J. Li, R.H. Dashwood, Emerging crosstalk between long non-coding RNAs and Nrf2 signaling, Cancer Lett. 490 (2020) 154–164.
[71] Kurinna, S. and S. Werner, NRF2 and microRNAs: New but Awaited Relations. (1470-8752 (Electronic)).
[72] X. Cheng, C.H. Ku, R.C. Siow, Regulation of the Nrf2 antioxidant pathway by microRNAs: new players in micromanaging redox homeostasis, Free Radic. Biol. Med. 64 (2013) 4–11.
[73] M. Ashrafizadeh, et al., MicroRNA-mediated regulation of Nrf2 signaling pathway: implications in disease therapy and protection against oxidative stress, Life Sci. 244 (2020), 117329.
[74] Y. Wang, et al., Biological function and mechanism of lncRNA-MEG3 in Tenon's capsule fibroblasts proliferation: by MEG3-Nrf2 protein interaction, Biomed. Pharmacother. 87 (2017) 548–554.
[75] L. Wu, et al., LncRNA MEG3 promotes melanoma growth, metastasis and formation through modulating miR-21/E-cadherin axis, Cancer Cell Int. 20 (1) (2020) 12.
[76] P. Li, et al., LncRNA MEG3 repressed malignant melanoma progression via inactivating Wnt signaling pathway, J. Cell. Biochem. 119 (9) (2018) 7498–7505.
[77] J. Long, X. Pi, lncRNA-MEG3 suppresses the proliferation and invasion of melanoma by regulating CYLD expression mediated by sponging miR-499-5p, BioMed Res. Int. 2018 (2018), 2086564.
[78] A. Latina, et al., ΔNp63 targets cytoglobin to inhibit oxidative stress-induced apoptosis in keratinocytes and lung cancer, Oncogene 35 (12) (2016) 1493–1503.
[79] G.X. Wang, et al., ΔNp63 inhibits oxidative stress-induced cell death, including ferroptosis, and cooperates with the BCL-2 family to promote clonogenic survival, Cell Rep. 21 (10) (2017) 2926–2939.
[80] W. Yan, X. Chen, GPX2, a direct target of p63, inhibits oxidative stress-induced apoptosis in a p53-dependent manner, J. Biol. Chem. 281 (12) (2006) 7856–7862.
[81] P. Moi, et al., Isolation of NF-E2-related factor 2 (Nrf2), a NF-E2-like basic leucine zipper transcriptional activator that binds to the tandem NF-E2/AP1 repeat of the beta-globin locus control region, Proc. Natl. Acad. Sci. U. S. A. 91 (21) (1994) 9926–9930.
[82] S. Singh, et al., Calcineurin activates cytoglobin transcription in hypoxic myocytes*, J. Biol. Chem. 284 (16) (2009) 10409–10421.
[83] M. Jaganjac, et al., Induction of CMV-1 promoter by 4-hydroxy-2-nonenal in human embryonic kidney cells, Acta Biochim. Pol. 57 (2) (2010) 179–183.
[84] W. Bruening, et al., Activation of stress-activated MAP protein kinases up-regulates expression of transgenes driven by the cytomegalovirus immediate/early promoter, Nucleic Acids Res. 26 (2) (1998) 486–489.